IEEE Access
Multidisciplinary | Rapid Review | Open Access Journal

Received 12 January 2023, accepted 23 January 2023, date of publication 30 January 2023, date of current version 2 February 2023.

Digital Object Identifier 10.1109/ACCESS.2023.3240465

RESEARCH ARTICLE

Design and Control of a Novel Detachable Driving Module for Electrification of Manual Wheelchairs

DONGYOUNG LEE AND SOONKYUM KIM, (Member, IEEE)
Center for Healthcare Robotics, Korea Institute of Science and Technology, Seoul 02792, South Korea

Corresponding author: Soonkyum Kim (kim.soonkyum@kist.re.kr)

This work was supported in part by the Korea Medical Device Development Fund Grant, funded by the Korea Government (the Ministry of Science and ICT, the Ministry of Trade, Industry and Energy, the Ministry of Health and Welfare, the Ministry of Food and Drug Safety), under Project 1711138428 and Project KD000198G0001053; and in part by the Korea Institute of Science and Technology (KIST) Institutional Program under Grant 2E32272.

ABSTRACT We developed a detachable electric module that converts a manual wheelchair into an electric wheelchair. The existing electric module requires several parts to be fastened to the wheelchair, which complicates its assembly. In addition, because the overall size of the wheelchair increases after its assembly and the turning radius increases compared to the manual wheelchair, controlling the wheelchair becomes difficult for the user. To compensate for these shortcomings, a new type of electric module composed of two omni-wheel driving units is proposed in this study. Because the two modules can independently move forward or backward and change directions, the same movement as that of the existing manual wheelchair is possible. In addition, a mechanism for easy attachment and detachment is proposed and its versatility is verified by mounting it on various wheelchairs. For the stable operation of the module, field-oriented control was applied, and the wheelchair was controlled for stably moving against external forces and ground disturbances according to the module mounting location. A driving test was conducted according to the mounting location of the developed module, and the proposed driving module and applied algorithm were verified through statistical analysis.

INDEX TERMS Detachable driving module, field-oriented control, omni-wheel, statistical analysis.

I. INTRODUCTION

Wheelchairs are a common means of transportation used by the disabled and elderly. Manual wheelchairs are widely used because they are lightweight, easy to operate, inexpensive, and elementary in form. In addition, if users cannot move their wheelchairs by themselves, caregivers can aid them. However, not all users have aid from others, and environmental conditions, such as inclinations and obstacles, challenge the use of manual wheelchairs.

Therefore, the demand for electric wheelchairs is increasing, and they are rapidly developing [1], [2], [3], [4]. These electric wheelchairs are classified into several types according to user requirements and usage environments [5], [6]. Therefore, various types of electric wheelchairs have been developed according to user needs [7], [8], [9], [10]. These electric wheelchairs are expensive, heavy, and complicated to operate, which necessitates training of the sick and elderly.

In addition, research on driving the wheelchairs through various interfaces according to the degree of user disability is still underway. Operation of such a wheelchair according to user intentions requires several sensors to be attached to different parts of the user [11], [12], [13]. These sensors cause the user some discomfort and make the prolonged use of a wheelchair difficult. In addition, the inaccuracy of the sensors and uncertainty of the user's intention may cause incorrect operation of the wheelchair. Several additional sensors must be combined for solving these problems. Such convergence requires high specification computing for signal processing and algorithm implementation. Moreover, the sensors mounted on the wheelchair limit user actions, make maintenance difficult, and shorten the operation time of the wheelchair because of battery limitations [14], [15], [16], [17]. Therefore, popularizing these

The associate editor coordinating the review of this manuscript and approving it for publication was Jingang Jiang.

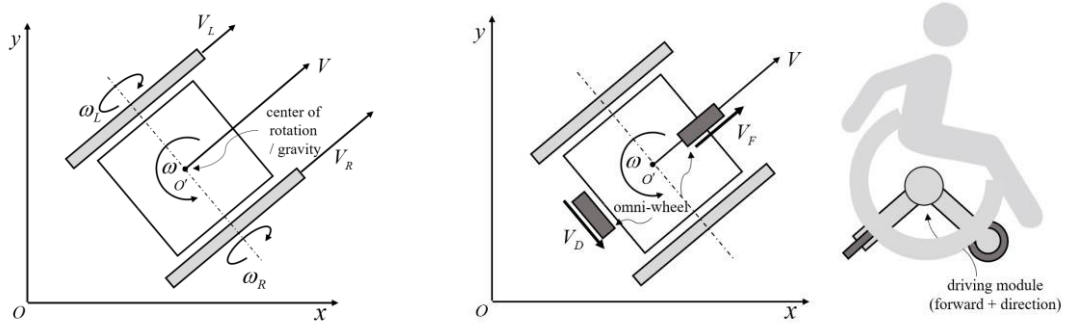

FIGURE 1. Existing manual wheelchairs and wheelchairs with driving modules. (a) Driving methods of existing manual wheelchairs, (b) Driving methods of the proposed detachable module. The detachable modules implement the same movements as existing manual wheelchairs.

types of wheelchairs is difficult because they are function focused rather than user centered.

The most basic and popular electric wheelchair has the functions of forward/backward motion and direction change. However, the movement of this electric wheelchair gets restricted in case of exhaustion of the battery if it is not manually switched. These wheelchairs are specialized only for outdoor driving. The large volume of these wheelchairs causes difficulties in operating them in a narrow corridor and inconvenience to the user and other people.

To overcome these shortcomings, a mountable electric module was developed for manual wheelchairs. However, because this module is mounted in front of the wheelchair and controlled by a steering, it increases the volume and radius of rotation [18]. Modules that can be mounted on the rim of the wheelchair for directly turning the wheel and achieving propulsion are also available [19]. However, they require multiple accessories, and the number of wheelchairs suitable for such mounting is limited. Such a driving module installed on a manual wheelchair is generally attached to an individual wheelchair. The module developed by Permobile has a single actuator attached to the rear of the wheelchair. Sudden emergency braking is difficult and the direction is changed manually. Additional accessories and user strength are required; therefore, it is not suitable for all users [20].

Many types of electric and manual wheelchairs have been developed, and various types of wheelchairs are expected to continue to be developed according to user environments and needs [1], [21].

However, investigations on developing an easily detachable indoor driving module are limited. Therefore, in this study, a detachable driving module converting a manual wheelchair into an electric wheelchair was developed. The contributions of this study are as follows:

- A module designed in this study has a novel structure, which guarantees the mobility of a manual wheelchair.
- Modules that do not require structural changes in wheelchairs were designed.
- The design is compatible with multiple wheelchairs and is easy to attach and detach.
- Driving assistance and control algorithms were developed for stable driving and safety.
- The performance of the driving module was validated through driving experiments and statistical analysis.

The configuration of the driving system and design of the electric and mechanical parts of the driving module are described in Section II. In Section III, the algorithm and controller design are described. The proposed system was experimentally verified, as discussed in Section IV. The results of statistical analysis based on the experimental data and future research plan are presented in Section V. The conclusions is discussed in Section VI.

II. SYSTEM CONFIGURATION

A. DRIVING MODULE DESIGN

The existing electric wheelchairs use at least three omnidirectional or mecanum wheels for realizing omnidirectional driving [22], [23], [24]. For these wheelchairs, the arrangement of the wheels and driving of each wheel must be considered for forward/backward movements and changing the direction. However, a general manual wheelchair has a differential-driving method, rotational motion, and straight motion. Therefore, most driving modules with two degrees-of-freedom move forward and backward at speed V and change direction at angular speed ω using the difference between the velocities V_L and V_R of both wheels in a two-wheel differential method, as shown in Fig. 1a. The majority of electric wheelchairs move in this manner. In this study, a type of driving using two omniwheels, as shown in Fig. 1b, is proposed. The module independently moves forward/backward (V_F) and changes direction (V_D). In addition, by separating the role of the driving unit, the driving module was designed by considering the driving and rotational forces required for driving.

The driving module is designed by dividing it into a forward/backward (left) and direction-change (right) driving

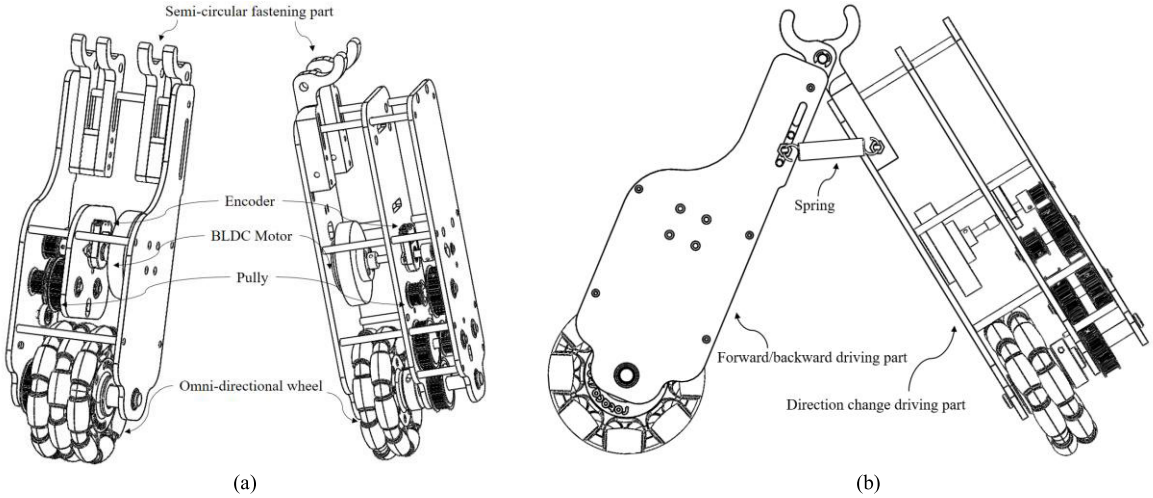

FIGURE 2. The driving module consists of two driving parts. (a) Forward/backward (left) and direction change (right) driving parts, (b) Side view of combined driving module.

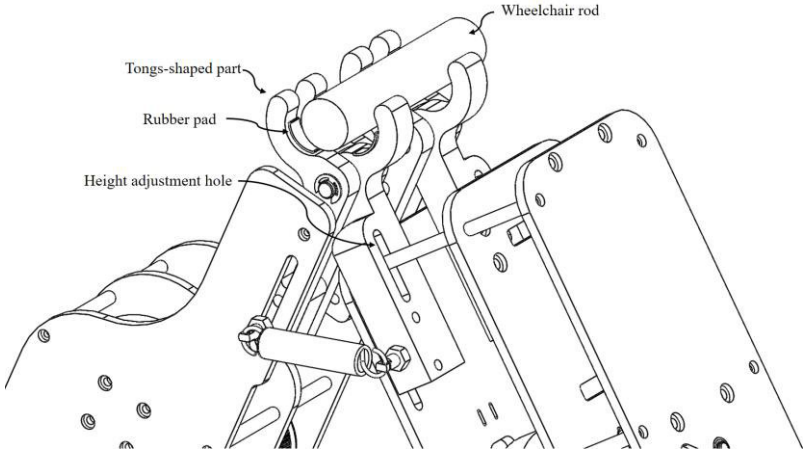

FIGURE 3. Tong-shaped part: Because of the weight of the wheelchair, the fastening part grabs the rod, and the driving module is fixed.

parts, as shown in Fig. 2a, consisting of semicircular fastening parts, each of which was connected by a pin to act as a driving module. Each driving unit consisted of a motor and pulley timing belt. The forward/backward driving part consisted of three pulley timing belts with a reduction ratio of 18.9:1. The motor exhibited a maximum speed of approximately 6 km/h with an application of 36 V.

The direction-change driving part exhibited a similar overall structure and four pulley timing belts. In addition, the direction was changed at low speeds, and the reduction ratio was 41:1 for stable turning. Therefore, its maximum mechanical speed was 1.61rad/s. However; however, unlike the forward/backward driving part, its speed was limited considering the user safety. As shown in Fig. 2b, these driving parts consist of a semicircular fastening part for coupling with each other and a wheelchair, and they are connected to a spring for creating a driving module.

B. ATTACHMENT TO AND DETACHMENT FROM THE WHEELCHAIR

In this study, a driving module consisting of semicircular fastening components was designed for facilitating its mounting on various types of wheelchairs. As shown in Fig. 3, each semicircular fastening part is joined in opposite directions to form tong-like shapes. As shown in Fig. 2b, when the module is not fastened to the wheelchair, the tongs open because of the force of the spring. The fastening of the wheelchair presses the fastening parts, the tong-shaped parts grab the rod of the wheelchair, and the module is firmly joined. Conversely, if the wheelchair is lifted for separation, the tong-shaped parts open using the restoring force of the spring, making separation easy.

In addition, after installing the module, the wheels of the module have to connect with the ground and push it. Therefore, the grip of the wheel is important. Because the gap between the rod and tong-shaped parts of the wheelchair

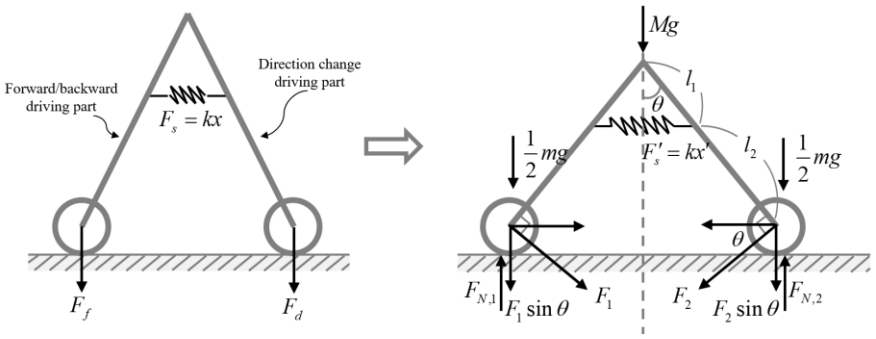

FIGURE 4. Grip force by wheelchair and driving module. When a wheelchair is placed on the driving module, the grip force of it increases due to the weight of the wheelchair and spring force.

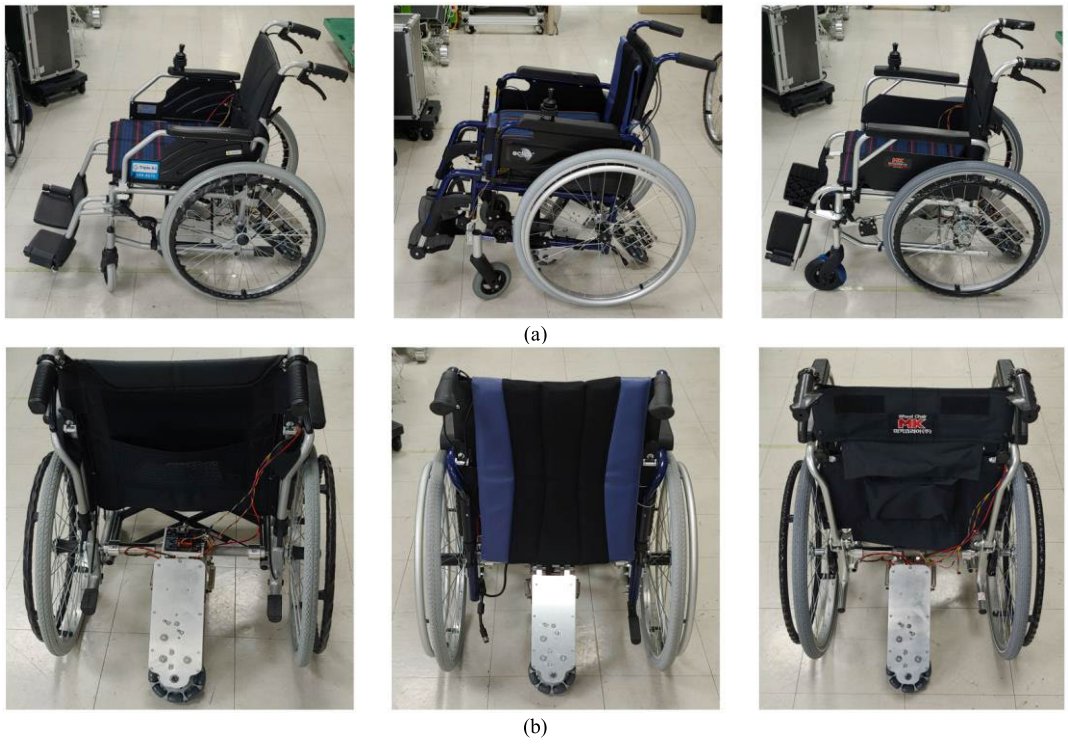

FIGURE 5. Developed driving module applied to various wheelchair types and sizes. The developed driving module was installed on three types of wheelchairs and its compatibility was verified. It is easy to attach and detach because of the tongs-shaped connection part. (a) side view, (b) rear view.

affects the contact and pressing force on the ground, a rubber pad was inserted between them. The force with which the two driving parts press on the ground can be obtained if the weights of the wheelchair and driving module are Mg and mg, respectively, and the force with which the module retracts because of the spring is F_s'.

The weight difference between the two parts of the module is extremely small compared with the weight of the wheelchair pressing against it; therefore, the weights of the two parts are assumed to be the same. If the position of the spring connected to each part is the same, it can be simplified as shown in Fig. 4. If the spring constant is k and its displacement is x', the forces acting on the two parts of the module are F_1 and F_2, respectively. Assuming that the weight of the wheelchair is equally distributed between the wheel of the wheelchair and module, the forces F_f and F_d for gripping can be expressed as $\frac{l_1}{2l_2}\left(kx'+mg+\frac{Mg}{2}\right)$. In addition, considering the weights of the user and wheelchair, F_f and F_d press the ground with a greater force. Thus, when the module was installed, driving was stable. $F_{N,1}$ and $F_{N,2}$ are the reaction forces exerted on the ground by the wheelchair, driving module, and spring.

Several types of manual wheelchairs differ in height owing to the size of the wheels. However, the developed driving module can be applied to various wheelchairs because of its tong-shaped part. The wheelchairs to which this module was applied are illustrated in Fig. 5. The module was stably mounted even if the height of the wheelchairs differed.

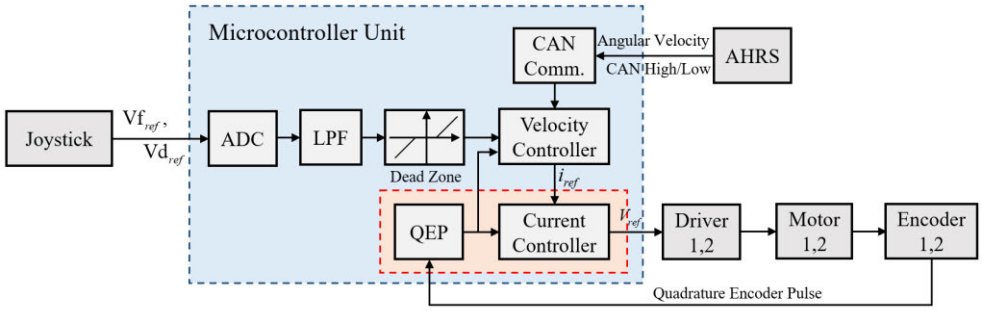

FIGURE 6. Block diagram of the entire system.

C. MOTOR AND ELECTRIC PART CONFIGURATION

Considering the size of the driving module, a flat-type brushless direct-current (BLDC) motor without a Hall sensor was used. These motors are mainly used in remotely controlled products such as drones because of their high performance and small size. The BLDC motor is driven by a three-phase inverter, and the position of the rotor is divided into six sections for commutation. When the rotor rotates and is positioned in each section, commutation must be performed. A Hall sensor is required for determining the rotor position [25]. For determining the rotor position for a motor without a Hall sensor, a sensor-less control for estimating rotor position has been studied [26], [27]. In this control, initial driving is essential for estimating the position of the rotor. When this control method is used for driving a wheelchair, the initial driving while the user is on board is unsuitable because it can cause an accident. Thus, field-oriented control (FOC), which does not require initial driving and can generate stable torque even at a low speed, was applied [28]. To apply FOC, knowing the electric angle of the motor is necessary; therefore, an additional encoder was installed.

The entire system was operated at 36 V, and the motor speed constant and thrust of the forward/backward drive module were 120 KV (rpm/v) and 12 kgf, respectively. At 36 V, the system had a maximum speed of 4320 rpm. However, in the case of a direction change module that does not require high speed and large force, the motor speed constant and thrust of the forward/backward drive module were 115 KV and 5 kgf, respectively. Fig. 6 shows the configuration of the electric system, where a microcontroller unit (MCU) independently controls the two motors. Therefore, the driving module is combined with two motor drivers, receives the encoder signal for controlling the FOC, and receives the attitude and heading reference system (AHRS) signal for processing the driving assistance algorithm. The red dotted line in Fig. 6 represents the current control loop where the FOC algorithm is applied. The wheelchair was driven using a joystick. The microcontroller receives the voltage value of the joystick through an analog-to-digital converter (ADC) and processes the noise through a low-pass filter. AHRS data were collected through controller area network (CAN) communication for controlling the posture of the wheelchair.

III. CONTROL CONFIGURATION

In the control system developed in this study, an MCU controlled the two motors. The controller adjusted six pulse-width modulation (PWM) signals and applied them to the motor driver. The motor driver applied voltage to the motor. An FOC was applied to drive the motor. For smooth driving and control performance of the motor, the PWM frequency was 50 kHz, and the frequencies of the current and speed controls were set to 25 and 2.5 kHz, respectively.

A. FIELD-ORIENTED CONTROL

Because the magnetization direction of the permanent magnet of a typical BLDC motor is radial, the back electromotive force (EMF) appears as a trapezoidal waveform. To drive with a trapezoidal back EMF, the same voltage as that of the back EMF was applied according to the rotor position, and sensorless control was applied depending on the presence or absence of the Hall sensor. This control is based on the zero-crossing algorithm for determining the position of the rotor; therefore, the initial driving is required. However, a motor without a Hall sensor was used in this study. To ensure the safety of wheelchair users, the motor must be controlled without initial driving. A control method that can solve this problem is FOC, which independently controls the current that generates the torque and magnetic flux of the motor. This method is generally used for permanent magnet synchronous motors (PMSMs) [28]. This is because the magnetization direction of the PMSM magnet is parallel. Consequently, the back EMF is sinusoidal [29]. This control technique drives the motor by applying a sinusoidal current based on rotor position information and phase current. The back EMF of the motor of the developed driving module approximates a sine wave; thus, the FOC is applied to the module [30].

Fig. 7. shows a block diagram of the FOC. The two-phase currents of the motor were measured and converted into two DC component currents through the Clarke and Park transforms [31]. Therefore, from a control point of view, for the control of the motor current, the reference input of the MCU

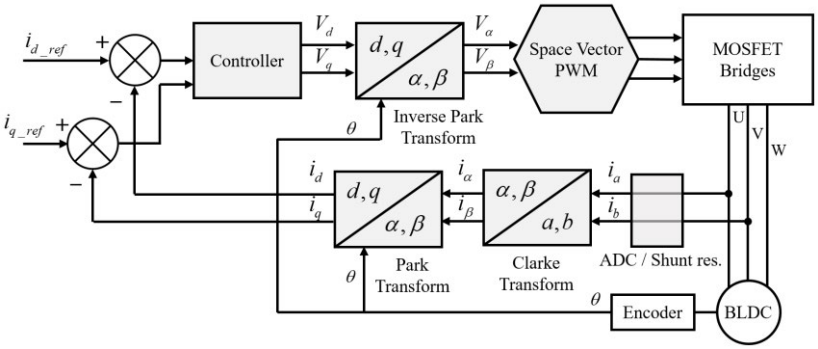

FIGURE 7. Block diagram of FOC for motor control of the module.

was the DC current, not the two-phase currents, which is easy to control because the controller follows the DC current value.

The currents i_a, i_b, and i_c measured by the motor can be expressed as $i\times \sin(\omega t)$, $i\times \sin(\omega t + 2\pi/3)$, and $i\times \sin(\omega t - 2\pi/3)$, respectively. These currents can be converted into two-phase currents with a phase difference of 90° using the Clarke transform. These phase currents are i_α and i_β and can be converted into two DC component currents (i_d and i_q) through the position information of the rotor and Park transform.

Because i_d and i_q respectively generate magnetic flux and torque, they are used as shown in Fig. 7; however, because the magnetic flux is not considered in the actual motor control, only i_q is input and the current is controlled.

The MCU performs an inverse Park transform on the output of the current controller, generates space vector PWM signals, and applies them to the metal–oxide–semiconductor field-effect transistor (MOSFET) bridges of the motor driver.

Fig. 8 shows the result of the current of the motor and its conversion at no load. At this time, the maximum output current of the motor driver is ±16.5 A, which is reduced to -1.0 to 1.0. The actual current was sinusoidal, as shown in Fig. 8a. The output current of the Park transform was in DC form, as shown in Fig. 8c. The space vector PWM output shown in Fig. 8d confirms that FOC stably drove the BLDC motor used in the module. Speed tracking of the motor was confirmed by applying the motor speed (-1.0–1.0) as a step input (see Fig. 8e). The motor wheel followed the speed profile through the control when it was applied to the driving module, as shown in Fig. 8f.

B. DRIVING MODULE CONTROL AND DRIVING ASSISTANCE ALGORITHM

Driving a wheelchair using a joystick can damage the driving module and mechanical structure because of sudden starting and braking, causing safety concerns.

The MCU controls the motor by generating a real-time speed profile for the command value of the joystick. In addition, a misalignment between the central axis of the wheelchair and module or the condition of the ground affects straight movement and driving performance of the wheelchair. This can cause problems because the wheelchair does not operate as intended by the user. Therefore, in this study, a dead zone was set for the direction-change command value of the joystick. If this value is outside the dead zone, the drive module follows it; otherwise, the MCU intervenes and controls the direction change module for straight driving. In other words, when the user drives straight, the controller detects the orientation of the wheelchair, responds to the disturbance, and follows the angular velocity of the yaw axis to 0.

IV. EXPERIMENTAL VALIDATION

A. EXPERIMENTAL METHOD

As mentioned in Section II, the driving module developed in this study is easily attachable and detachable. Mounting it on the central axis of the wheelchair rim is important for stable driving. However, mounting it at the center is difficult for users, and incorrect mounting affects the driving. In addition, the slope of the floor or condition of the ground induces an external force that acts on the wheelchair. A force is generated for rotating the wheelchair, depending on the mounting position of the driving module. Assuming that the center of gravity of the wheelchair is at its center of rotation, as shown in Fig. 1, the torque that affects the rotation of the wheelchair is expressed as F × r depending on the location of the driving module. Here, r is the distance between the center of rotation and module, and force F pulls the wheelchair forward. After the user boards the wheelchair, the vertical force acting on the module changes owing to the movement of the center of gravity according to the user's posture or behavior. These uncertainties affect driving; in particular, the torque according to the position of the driving module is the main factor hindering the straight motion of the wheelchair.

The driving module for indoor driving was tested on a flat ground for determining whether the wheelchair could stably move in a straight line even under the influence of different environments and disturbances. An attempt was made for validating the suitability of the driving module for manual wheelchairs.

The experiment was conducted with and without the installed module and wheelchair orientation control

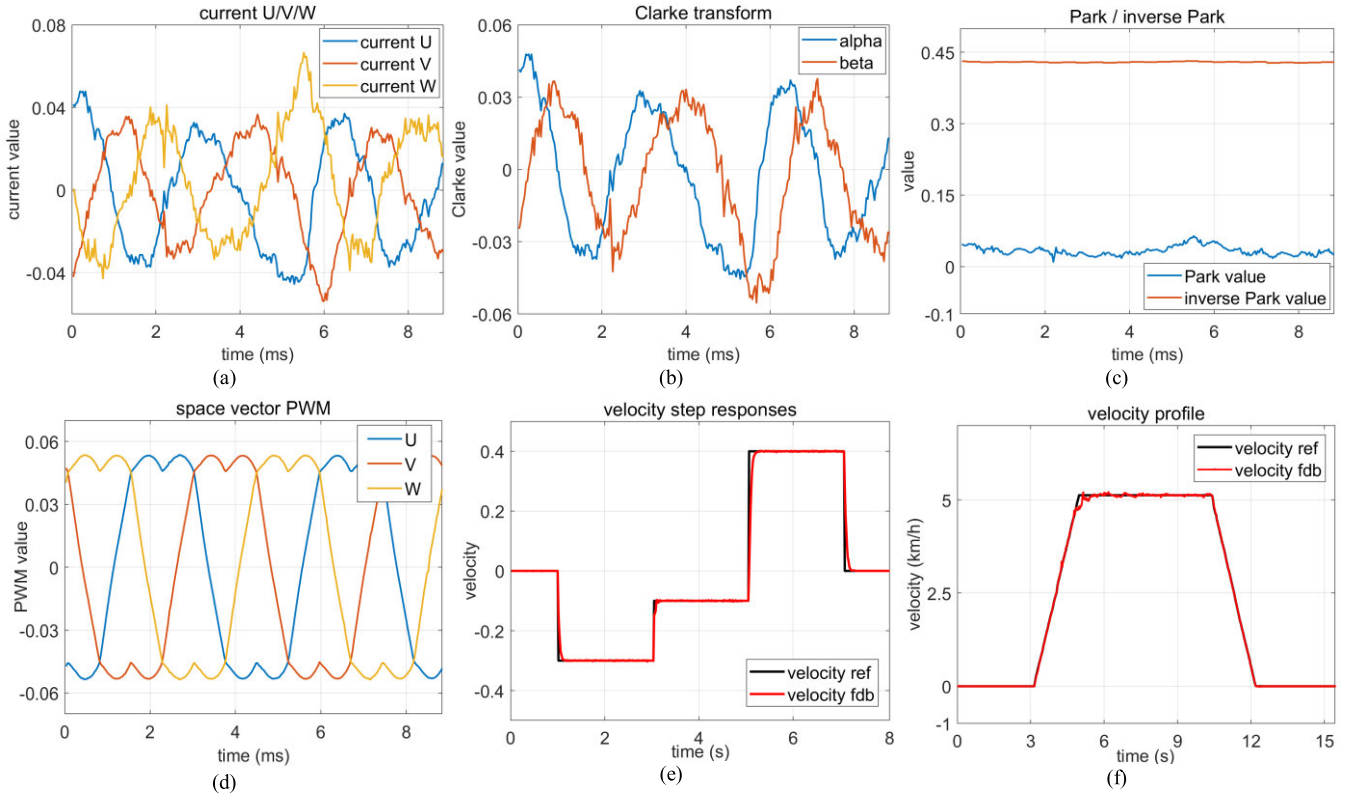

FIGURE 8. Output values for each step of FOC algorithm and motor velocity control: (a) 3-phase currents of the motor, (b) current converted through Clarke transform, (c) current converted through Clarke transform is converted into Park value and inverse Park value through park transform and inverse park transform, (d) output space vector PWM through inverse Park value, (e) motor velocity tracking result for step input, (f) motor velocity tracking result for velocity profile.

TABLE 1. Average and standard deviation of the sum of angular velocities with and without algorithm.

	Algorithm O					Algorithm X				
	A10	A8	A6	A4	A2	A0	NA6	NA4	NA2	NA0
Avg.	2.469	2.516	2.488	2.477	2.884	2.832	64.813	59.115	51.786	42.965
Std.	0.932	0.573	1.010	0.738	1.383	0.924	27.958	27.258	34.372	26.671

algorithm. In the experiment, the user was assumed to generate an inaccuracy from 0 mm (center point) to 10 mm (maximum) when the module was mounted. Therefore, six points were set at intervals of 2 mm to the left of the center of rotation of the wheelchair, and 20 driving tests were conducted at each point.

Instead of using the joystick after the user boarded, the wheelchair followed the velocity profile. When no algorithm was used, a module was only mounted from 0 to 6 mm. This was because a module movement of $\geq$ 8 mm was not meaningful. At this time, the slip was not considered, and the test was conducted where the motor of the driving module had a constant speed of 90% of the maximum motor speed (approximately 2480 rpm) for 6 s, except for the acceleration/deceleration. The sum of the absolute values of the angular velocity was used as an index for evaluating the straight-line driving performance of the wheelchair against disturbances.

B. STATISTICAL ANALYSIS

The experimental results when the algorithm was applied (A0–A10) and not applied (NA0–NA6) are listed in Table 1. With no algorithm (NA), straight line motion was difficult, even when the module was installed at the center. Therefore, the test according to the change in the module mounting position was not meaningful.

The average and standard deviation of the sum of the angular velocities are listed in Table 1. The sum of angular velocities includes the left and right rotations of the wheelchair. With the algorithm, the mean of the sum ranged from approximately 2.5 to 3. Without the algorithm, it ranged from approximately 40 to 65.

To analyze the above results, a null hypothesis that there was no difference in straight-line driving performance between the groups was established. The p-value, the probability of not rejecting the null hypothesis, is usually set to 0.05. However, in the above experiment, many null

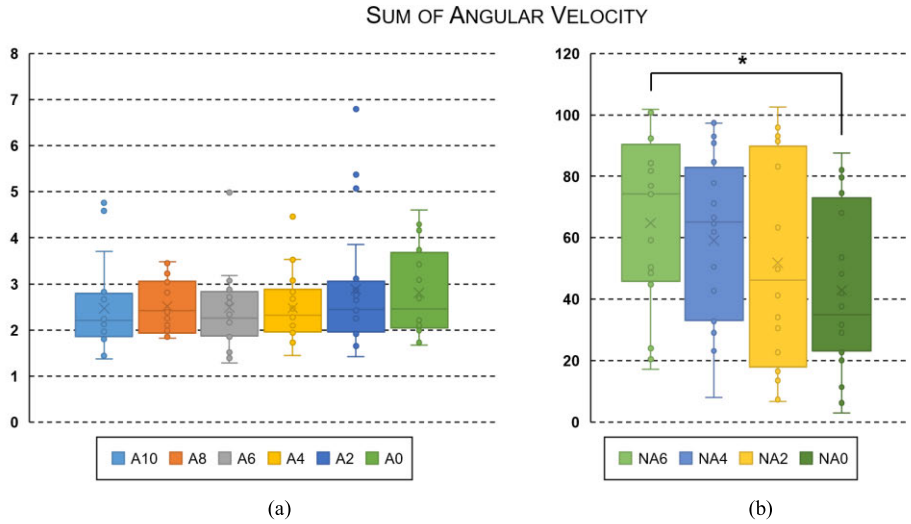

FIGURE 9. Box- and -whisker plot of the sum of the angular velocities, (a) with algorithm, (b) without algorithm.

hypotheses were established because multiple comparisons were performed. Therefore, as the probability of an error increased, the p-value was adjusted from 0.05 to 0.0278 using a false discovery rate (FDR), a post-processing method [32]. Using this changed p-value, the performances with and without the algorithm were compared, and the performance according to the mounting position of the driving module was compared.

C. EXPERIMENT RESULTS

Fig. 9 shows a box-and-whisker plot of the sum of the angular velocities of the 20 driving tests in the experiment. When the algorithm was applied, as shown in Fig. 9a, except for the outlier values, the values from the first through third quartiles (Q1—Q3) were approximately 24. The median value was 2–3. However, in the case of the straight test without algorithm, as shown in Fig. 9b, the values of Q1 and Q3 according to the module position were widely distributed, that is, the standard deviation was quite large, and the median value increased as the module moved away from the center.

A comparison of the sum-of-angular-velocity values confirmed the difference between the cases with and without the algorithm. The final coordinates and trajectory of the wheelchair were determined based on the average values listed in Table 1, as shown in Fig. 10a. In the experiment, for the same speed and time, the trajectory of the wheelchair was obtained when the sum of the angular velocities was 2.5, 5, 10, and 40–70. The final coordinates of the wheelchair for A0–A10 and NA0–NA6 are shown in the figure.

Using the trajectory shown in Fig. 10a, the maximum curvature of the wheelchair can be estimated according to the sum of angular velocities. However, in the case of the module with the algorithm, the actual wheelchair trajectory exhibited a much smaller curvature than the estimated trajectory. The trajectory to which the algorithm was applied is shown in Fig. 10b, and the positions of the modules were 6 and 8 mm from the center. There was no difference in the results according to the module location.

D. CERTIFICATION RESULTS

The straight-line driving performance of the driving module was confirmed through the experiment, and when the module was applied to a wheelchair, we requested verification from an external certification authority after evaluating its performance. Three tests were conducted on payload, velocity, and gradability. The performance was certified; the certification results are listed in Table 2.

V. DISCUSSION

A. DISCUSSION OF RESULTS

To evaluate the performance of the driving module, a test was conducted by varying the mounting position of the module. Twenty iterations were conducted with and without the algorithm, and an analysis of variance (ANOVA) was performed on the results. Each case was divided into equal and unequal variances through an f-test, and a t-test was performed for each case, as listed in Table 3. The p-value was set to 0.0278 using FDR. As summarized in Table 3, the t-test values for the sum-of-angular-velocity values of A10 and A8 were 8.480E-01. As this was larger than the adjusted p-value of 0.0278, the null hypothesis could not be rejected. Therefore, no significant difference existed between A10 and A8.

Additionally, the null hypotheses of A10 and A6–A0 could not be rejected. Multiple comparisons were performed for each experiment from A10 to A0. In all cases, this hypothesis was not rejected, as indicated in red. This shows that the module with the algorithm achieved the same performance at any position between 10 mm and center. The p-values with and without the algorithm were significantly less than 0.0287.

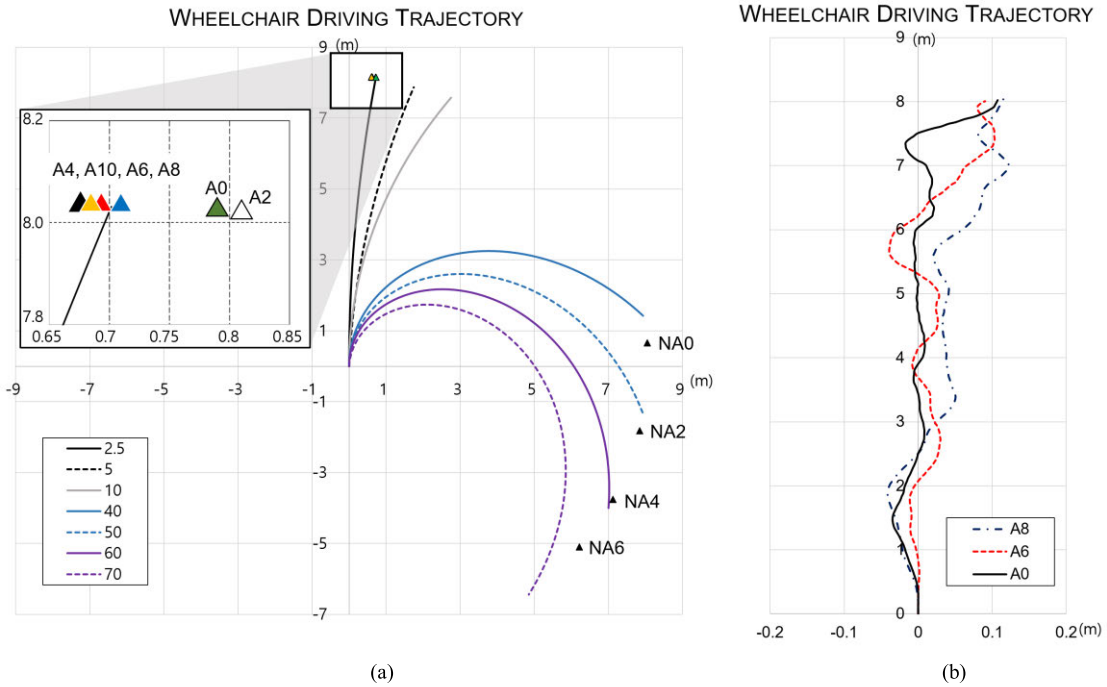

FIGURE 10. Trajectory and final coordinate value according to the mounting position of the wheelchair module. (a) compare the coordinates and trajectories of the wheelchair with and without algorithm, (b) actual trajectory of the wheelchair with algorithm.

TABLE 2. Test certification results through verification agency.

Items	Test / Inspection Methods and Criteria		Test/Inspection Results and Remarks	Judgment (Pass, Fail and N/A)
	Methods	Criteria		
Payload	Verification that it can move more than 5m with a payload of 100kg.	100kg	It can move forward more than 5m with a payload of 100 kg	Pass
Velocity	Verification that it can move at 5km/h or more with a payload of 60kg or more.	5km/h	6.12 km/h	Pass
Gradability	Verification that it can climb a 6° of slopes with a payload of 60kg or more.	6°	It can climb 6° of slopes with a payload of 78 kg.	Pass

Verification agency: Korea Testing Laboratory (http://ktl.re.kr)
Report No: 22-075912-01-1

TABLE 3. Result of t-test.

t-test	A10	A8	A6	A4	A2	A0	NA6	NA4	NA2	NA0
A10		8.480E-01	9.494E-01	9.765E-01	2.722E-01	2.232E-01	5.551E-09	1.705E-08	3.768E-06	1.837E-06
A8			9.159E-01	8.514E-01	2.817E-01	2.027E-01	5.588E-09	1.717E-08	3.805E-06	1.857E-06
A6				9.666E-01	3.076E-01	2.683E-01	5.588E-09	1.717E-08	3.791E-06	1.852E-06
A4					2.542E-01	1.866E-01	5.544E-09	1.702E-08	3.769E-06	1.836E-06
A2						8.892E-01	6.248E-09	1.935E-08	4.240E-06	2.136E-06
A0							6.097E-09	1.886E-08	4.156E-06	2.078E-06
NA6								5.180E-01	1.964E-01	1.572E-02
NA4									4.595E-01	6.526E-02
NA2										3.678E-01
NA0										

A difference existed in their performances, as revealed by the ANOVA, as shown in Fig. 10.

Moreover, as shown in Fig. 9b, which is a box-and-whisker plot of the sum-of-angular velocity for the case without

the algorithm, the median value increased according to the mounting position. However, based on ANOVA, because the null hypothesis could not be rejected, no difference between them was observed, even if the module gradually moved away from the center (NA0). This resulted from the influence of various disturbances and misalignment of the module. However, the ANOVA results for NA0 and NA6 were smaller than the adjusted p-value of 0.0287. Thus, a difference was observed only when the module was more than 6 mm away from the center. Based on these results, the drive module developed in this study can be easily mounted on a wheelchair and has stable driving performance.

B. LIMITATIONS AND FUTURE WORK

Because this study was conducted for module development, only tests for driving on flat ground and slopes were conducted (not for driving on curves and environments with obstacles). This module was developed for indoor environments, in hospitals or nursing facilities where wheelchairs are frequently used. However, these environments also have curved corridors and obstacles. Therefore, as a follow-up to this study, a module that recognizes such environments as curved corridors and obstacles should be researched for assisting driving of a wheelchair.

VI. CONCLUSION

An electric drive module that could be attached to and detached from a wheelchair was designed and manufactured. The limitations of the existing electric wheelchairs and modules were identified and reflected in the design of this developed module. In addition, a new type of detachable mechanism was developed considering its compatibility with various wheelchairs, and the module was miniaturized for user convenience. For this purpose, a controller for the stable motor rotation of the driving part was configured using a flat BLDC motor instead of a general one. Subsequently, an algorithm using an inertial sensor was applied to assist the wheelchair with driving. Subsequently, an experiment was conducted by installing the module on an actual wheelchair. In addition, the performance and effectiveness of the modules were validated using statistical analysis.

REFERENCES

[1] J. Leaman and H. M. La, "A comprehensive review of smart wheelchairs: Past, present, and future," *IEEE Trans. Human-Mach. Syst.*, vol. 47, no. 4, pp. 486–499, Aug. 2017, doi: 10.1109/THMS.2017.2706727.

[2] C. Wang, M. Xia, and M. Q.-H. Meng, "Stable autonomous robotic wheelchair navigation in the environment with slope way," *IEEE Trans. Veh. Technol.*, vol. 69, no. 10, pp. 10759–10771, Oct. 2020, doi: 10.1109/TVT.2020.3009979.

[3] J. L. Candiotti, B. J. Daveler, D. C. Kamaraj, C. S. Chung, R. Cooper, G. G. Grindle, and R. A. Cooper, "A heuristic approach to overcome architectural barriers using a robotic wheelchair," *IEEE Trans. Neural Syst. Rehabil. Eng.*, vol. 27, no. 9, pp. 1846–1854, Sep. 2019, doi: 10.1109/TNSRE.2019.2934387.

[4] H. Wang, Y. Sun, and M. Liu, "Self-supervised drivable area and road anomaly segmentation using RGB-D data for robotic wheelchairs," *IEEE Robot. Autom. Lett.*, vol. 4, no. 4, pp. 4386–4393, Oct. 2019, doi: 10.1109/LRA.2019.2932874.

[5] M. Callejas-Cuervo, A. X. González-Cely, and T. Bastos-Filho, "Control systems and electronic instrumentation applied to autonomy in wheelchair mobility: The state of the art," *Sensors*, vol. 20, no. 21, p. 6326, Nov. 2020, doi: 10.3390/s20216326.

[6] M. Khalili, G. Kryt, H. F. M. Van der Loos, and J. F. Borisoff, "A comparison between conventional and terrain-specific adaptive pushrim-activated power-assisted wheelchairs," *IEEE Trans. Neural Syst. Rehabil. Eng.*, vol. 29, pp. 2550–2558, 2021, doi: 10.1109/TNSRE.2021.3132644.

[7] Y. Munakata and M. Wada, "A novel step climbing strategy for a wheelchair with active-caster add-on mechanism," in *Proc. IEEE/RSJ Int. Conf. Intell. Robots Syst. (IROS)*, Sep. 2015, pp. 6324–6329.

[8] K. Goher, A. Al-Yahmadi, and I. Bahadur, "Kinematic analysis of the sit-to-stand mechanism of a reconfigurable wheelchair," in *Proc. IEEE EMBS Conf. Biomed. Eng. Sci. (IECBES)*, Kuala Lumpur, Malaysia, Dec. 2016, pp. 788–791, doi: 10.1109/IECBES.2016.7843558.

[9] K. Sasaki, Y. Eguchi, and K. Suzuki, "Stair-climbing wheelchair with lever propulsion control of rotary legs," *Adv. Robot.*, vol. 34, no. 12, pp. 802–813, Jun. 2020, doi: 10.1080/01691864.2020.1757505.

[10] J. Candiotti, B. Daveler, S. Sivakanthan, G. Grindle, R. Cooper, and R. Cooper, "Curb negotiation with dynamic human–robotic wheelchair collaboration," *IEEE Trans. Human-Mach. Syst.*, vol. 52, no. 1, pp. 149–155, Feb. 2022, doi: 10.1109/THMS.2021.3131672.

[11] A. S. Kundu, O. Mazumder, P. K. Lenka, and S. Bhaumik, "Hand gesture recognition based omnidirectional wheelchair control using IMU and EMG sensors," *J. Intell. Robotic Syst.*, vol. 91, nos. 3–4, pp. 529–541, Sep. 2018, doi: 10.1007/s10846-017-0725-0.

[12] P. Chawda, A. Sridhar, A. G. Mishra, H. Dedhia, M. Kambli, and S. Kadge, "Design and implementation of hybrid BCI based wheelchair," in *Proc. 2nd Int. Conf. Smart Electron. Commun. (ICOSEC)*, Trichy, India, Oct. 2021, pp. 557–565, doi: 10.1109/ICOSEC51865.2021.9591796.

[13] Z. Li, S. Zhao, J. Duan, C.-Y. Su, C. Yang, and X. Zhao, "Human cooperative wheelchair with brain-machine interaction based on shared control strategy," *IEEE/ASME Trans. Mechatronics*, vol. 22, no. 1, pp. 185–195, Feb. 2017, doi: 10.1109/TMECH.2016.2606642.

[14] R. Arnay, J. Hernández-Aceituno, J. Toledo, and L. Acosta, "Laser and optical flow fusion for a non-intrusive obstacle detection system on an intelligent wheelchair," *IEEE Sensors J.*, vol. 18, no. 9, pp. 3799–3805, May 2018, doi: 10.1109/JSEN.2018.2815566.

[15] L. Devigne, M. Aggravi, M. Bivaud, N. Balix, C. S. Teodorescu, T. Carlson, T. Spreters, C. Pacchierotti, and M. Babel, "Power wheelchair navigation assistance using wearable vibrotactile haptics," *IEEE Trans. Haptics*, vol. 13, no. 1, pp. 52–58, Jan. 2020, doi: 10.1109/TOH.2019.2963831.

[16] D. Cojocaru, L. F. Manta, I. C. Vladu, A. Dragomir, and A. M. Mariniuc, "Using an eye gaze new combined approach to control a wheelchair movement," in *Proc. 23rd Int. Conf. Syst. Theory, Control Comput. (ICSTCC)*, Oct. 2019, pp. 626–631, doi: 10.1109/ICSTCC.2019.8886158.

[17] H. Luo, Z. Yang, P. Yin, J. O. Brooks, and B. Li, "Modeling and prediction of user stability and comfortability on autonomous wheelchairs with 3-D mapping," *IEEE Trans. Human-Mach. Syst.*, vol. 52, no. 6, pp. 1216–1226, Dec. 2022, doi: 10.1109/THMS.2022.3195775.

[18] UNAwheel. *UNAwheel Maxi Online User Manual*. Accessed: Jan. 29, 2023. [Online]. Available: https://maxi.unawheel.eu/manual

[19] TodoWORKS. *Todo-Drive*. Accessed: Jan. 29, 2023. [Online]. Available: https://have.todo-works.com/story/todo-drive

[20] Permobile. *Smartdrive*. Accessed: Jan. 29, 2023. [Online]. Available: https://hub.permobil.com/smartdrive

[21] L. Sang, M. Yamamura, F. Dong, Z. Gan, J. Fu, H. Wang, and Y. Tian, "Analysis, design, and experimental research of a novel wheelchair-stretcher assistive robot," *Appl. Sci.*, vol. 10, no. 1, p. 264, Dec. 2019, doi: 10.3390/app10010264.

[22] K. Shirai, H. Madokoro, and K. Sato, "Proximity sensing and movements of omnidirectional mobile electric wheelchair for autopilot," in *Proc. SICE Annu. Conf. (SICE)*, Sep. 2014, pp. 1296–1301.

[23] A. S. Kundu, O. Mazumder, P. K. Lenka, and S. Bhaumik, "Design and performance evaluation of 4 wheeled omni wheelchair with reduced slip and vibration," *Proc. Comput. Sci.*, vol. 105, pp. 289–295, Dec. 2016, doi: 10.1016/j.procs.2017.01.224.

[24] Y. Maeda, "Instruction recognition used gaze and EMG information for omni-directional wheelchair," in *Proc. IEEE Int. Conf. Fuzzy Syst. (FUZZ-IEEE)*, Jul. 2017, pp. 1–6.

[25] Y. Lee and J. Kim, "A novel enhanced inverted PWM driving scheme for three-phase BLDC motor drive," in *Proc. IEEE Int. Conf. Consum. Electron. Asia (ICCE-Asia)*, Jun. 2018, pp. 206–212.

[26] Y. Wang, X. Zhang, X. Yuan, and G. Liu, "Position-sensorless hybrid sliding-mode control of electric vehicles with brushless DC motor," *IEEE Trans. Veh. Technol.*, vol. 60, no. 2, pp. 421–432, Feb. 2011, doi: 10.1109/TVT.2010.2100415.

[27] J. S. Park, K.-D. Lee, S. G. Lee, and W.-H. Kim, "Unbalanced ZCP compensation method for position sensorless BLDC motor," *IEEE Trans. Power Electron.*, vol. 34, no. 4, pp. 3020–3024, Apr. 2019, doi: 10.1109/TPEL.2018.2868828.

[28] M. Abassi, A. Khlaief, O. Saadaoui, A. Chaari, and M. Boussak, "Performance analysis of FOC and DTC for PMSM drives using SVPWM technique," in *Proc. 16th Int. Conf. Sci. Techn. Autom. Control Comput. Eng. (STA)*, Monastir, Tunisia, Dec. 2015, pp. 228–233, doi: 10.1109/STA.2015.7505167.

[29] T. M. Jahns and W. L. Soong, "Pulsating torque minimization techniques for permanent magnet AC motor drives-a review," *IEEE Trans. Ind. Electron.*, vol. 43, no. 2, pp. 321–330, Apr. 1996, doi: 10.1109/41.491356.

[30] A. Bosso, C. Conficoni, D. Raggini, and A. Tilli, "A computational-effective field-oriented control strategy for accurate and efficient electric propulsion of unmanned aerial vehicles," *IEEE/ASME Trans. Mechatronics*, vol. 26, no. 3, pp. 1501–1511, Jun. 2021, doi: 10.1109/TMECH.2020.3022379.

[31] S. Chattopadhyay, M. Mitra, and S. Sengupta, "Clarke and park transform," in *Power Systems*. Dordrecht, The Netherlands: Springer, 2011, pp. 89–96, doi: 10.1007/978-94-007-0635-4_12.

[32] Y. Benjamini and Y. Hochberg, "Controlling the false discovery rate: A practical and powerful approach to multiple testing," *J. Roy. Stat. Society B*, vol. 57, no. 1, pp. 289–300, Aug. 1995, doi: 10.1111/j.2517-6161.1995.tb02031.x.

DONGYOUNG LEE received the M.S. and Ph.D. degrees from Yonsei University, South Korea, in 2013 and 2020, respectively. He is currently a Postdoctoral Researcher with the Korea Institute of Science and Technology. His research interests include robotics, hydraulic systems, embedded systems, and motion control.

SOONKYUM KIM (Member, IEEE) received the B.S. and M.S. degrees in mechanical engineering from Seoul National University, Seoul, South Korea, in 2002 and 2006, respectively, and the Ph.D. degree in mechanical engineering and applied mechanics from the University of Pennsylvania, in 2013.

From 2013 to 2014, he was a Postdoctoral Researcher at The Robotics Institute, Carnegie Mellon University. From 2015 to 2018, he worked as a Robot Controller Developer at Samsung Electronics. Since 2018, he has been with the AI Robotics Center, Korea Institute of Science and Technology. He is also serving as an Adjunct Professor with Yonsei University, as participating KIST-Yonsei Institutional Program of South Korea. His research interests include robotics, optimization, path planning, and machine learning.